SUPPORTING INFORMATION

Nanoarchitectonics of Glass Coatings for Near-Infrared Shielding: From Solid-State Cluster-Based Niobium Chlorides to the Shaping of Nanocomposite Films

Clément Lebastard,[a,b,‡] *Maxence Wilmet,*[b,a,c‡] *Stéphane Cordier,*[a,*] *Clothilde Comby-Zerbino,*[d] *Luke MacAleese,*[d] *Philippe Dugourd,*[d] *Tetsuo Uchikoshi,*[b,e] *Vincent Dorcet,*[a] *Maria Amela-Cortes,*[a] *Adèle Renaud,*[a] *Karine Costuas,*[a,*] *Fabien Grasset*[b,a]

[a] Univ Rennes, CNRS, ISCR (Institut des Sciences Chimiques de Rennes) – UMR 6226, F-35000 Rennes, France.

[b] CNRS – Saint-Gobain – NIMS, IRL 3629, Laboratory for Innovative Key Materials and Structures (LINK), National Institute for Materials Science, 1-1 Namiki, 305-0044 Tsukuba, Japan

[c] Saint-Gobain Research Paris, F-93300 Aubervilliers, France.

[d] Univ Lyon, Université Claude Bernard Lyon 1, ENS de Lyon, Institut des Sciences Analytiques, UMR 5280, 5 rue de la Doua, F-69100 Villeurbanne, France.

[e] Research Center for Functional Materials, National Institute for Materials Science (NIMS), 1-1 Namiki, Tsukuba, Japan.

* Emails: karine.costuas@univ-rennes1.fr; stephane.cordier@univ-rennes1.fr

I. Experimental Section

II. Computational study

I. Experimental section

Experimental procedures

*Synthesis of crude $K_4[\{Nb_6Cl^i_{12}\}Cl^a_6]$ (**1**).* The synthesis of $K_4[\{Nb_6Cl^i_{12}\}Cl^a_6]$ was done by solid-state reaction thanks to the reduction of the pentahalogenated ($NbCl_5$, Strem, 99.99 %) precursor by an excess of metallic niobium (Nb, Alfa Aesar, 99.8 %) in presence of alkaline salt (KCl, Alfa Aesar, 99 %)). The relative proportion of the synthesis was 4:2.8:7.5 (KCl:$NbCl_5$:Nb). 0.551 g of KCl (7.40 mmol), 1.399 g of $NbCl_5$ (5.18 mmol) and 1.288 g of Nb (13.87 mmol). The powder precursors were mixed together in an argon glovebox and put into a silica tube sealed under vacuum. The $K_4[\{Nb_6Cl^i_{12}\}Cl^a_6]$ phase was obtained after a heating treatment at 600 °C during 24 h, with a heating and cooling rate of 1 °C/min and 2 °C/min respectively. X-ray powder diffraction analysis of the powder revealed the presence of the desired $K_4[\{Nb_6Cl^i_{12}\}Cl^a_6]$ phase along with an excess of KCl and niobium powder. The structure of the $[\{M_6X^i_{12}\}X^a_6]^{4-}$ cluster unit is centered on a 2*a* Wyckoff position implying the C_{2h} local symmetry, while counter cations are located in an 8*j* general position. This as-prepared powder sample is named **1** thereafter in the text. Thanks to the difference in solubility between $K_4[\{Nb_6Cl^i_{12}\}Cl^a_6]$ and the by-products, mostly unreacted KCl and Nb, the synthesis yield could be determined. To do so, 1g of **1** was dissolved in dried acetone in a Schlenk flask under argon atmosphere, in order to remove KCl, Nb (metallic form), and traces of amorphous inorganic species that are hardly soluble. After 24 hours of stirring, the insoluble powder was recovered, dried and weighted. It corresponds to 37.5 ± 0.5 % by weight of **1** and consequently **1** contains 62.5 % ± 0.5 % of $K_4[\{Nb_6Cl^i_{12}\}Cl^a_6]$. The recovered powder was then poured in water and stirred for an extra 24 hours, to get rid of water-soluble impurities, mainly KCl. Following the same procedure, the recovered powder was recovered, dried and weighted. It corresponds to niobium powder and represents 15.5 ± 0.5 % by weight of **1**. Therefore, by subtraction, the soluble impurities in water correspond to 22.0 ± 0.5 % of **1**. The error bar of 0.5 % considers the error on the weight measurements. By-products determination was made several times with various batches of **1** to highlight reproducibility.

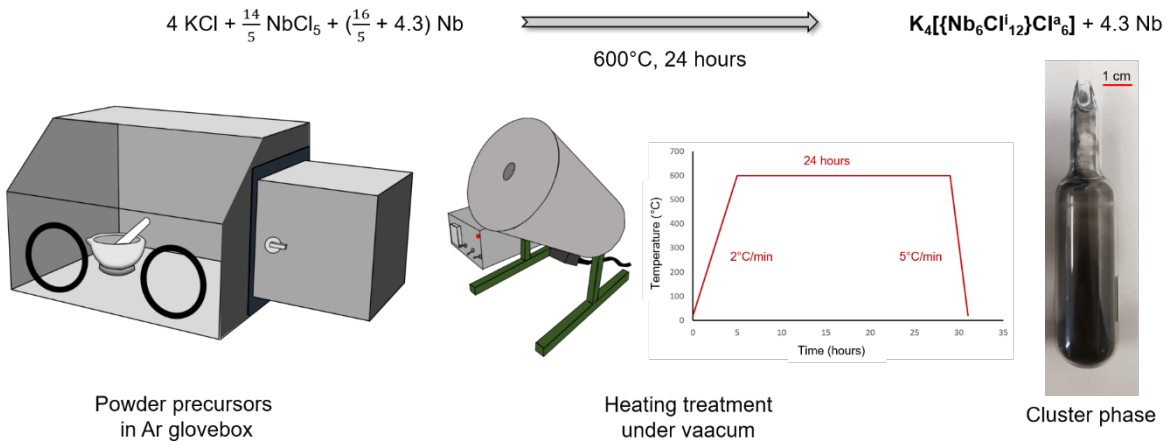

Scheme S1. Synthesis of crude phase $K_4[\{Nb_6Cl^i_{12}\}Cl^a_6]$.

Advantages and drawbacks of earlier published methods

The early published methods for the preparation of $K_4[\{Nb_6Cl^i_{12}\}Cl^a_6]$ consist in the reaction of the reduced halides Nb_3Cl_8 or Nb_6X_{14} with KCl under reducing atmosphere.[1] The reaction between KCl, Nb_3Cl_8 and Nb takes place at 800°C in a complex multi-compartmented device wherein the final $K_4[\{Nb_6Cl^i_{12}\}Cl^a_6]$ is collected in a niobium crucible. The reaction between KCl and Nb_6Cl_{14} takes place at 650°C in silica container during 4 days. Note that in this case, the precursor contains the preformed $\{Nb_6Cl^i_{12}\}$ cluster core. Fleming *et al.* developed another method which consists to reduce the $NbCl_5$ halide with niobium powder in the presence of KCl ($KCl:NbCl_5:Nb$ = 4:14/5:16/5) in a niobium container.[2] The reported reaction temperature is 850°C and the reaction time is 4-6 days for a rather low yield. Considering the low yield and/or the complexity of the solid-state reactions to obtain $K_4[\{Nb_6Cl^i_{12}\}Cl^a_6]$ published hitherto, this ternary halide was used only a few time as precursor of $\{Nb_6Cl^i_{12}\}$ cluster core for solution chemistry. The alternative method developed by Parsons *et al* involves the $Na_4[\{Nb_6Cl^i_{12}\}Cl^a_6]$ solid-state precursor instead of $K_4[\{Nb_6Cl^i_{12}\}Cl^a_6]$.[3] The preparation of $Na_4[\{Nb_6Cl^i_{12}\}Cl^a_6]$ is based on the reduction of $NbCl_5$ by a large excess of niobium powder in the presence of NaCl in silica container. For a stoichiometric reaction, the ($NaCl:NbCl_5:Nb$) ratio is (4: (14/5 = 2.8):(16/5 = 3.2) whereas the ($NaCl:NbCl_5:Nb$) ratio used by Parsons is (4:(14/5):13) meaning the use of a 4-fold excess of niobium. The reaction takes place at 800°C for (6 - 8 h) in silica container. In this work, we have optimized the synthesis of $K_4[\{Nb_6Cl^i_{12}\}Cl^a_6]$ in order to reach the lowest temperature reaction and in order to use a minimum excess of niobium.

*Synthesis of $[\{Nb_6Cl^i_{12}\}Cl^a_2(H_2O)^a_4]\cdot 4H_2O$ (**2**).* A protocol derived from that of Koknat and coworkers[1] was developed. 1.5 g of **1** were introduced in 10 ml of degassed water under argon. After 10 hours of stirring, the solution was decanted and filtered on a filter paper (thickness 0.15 mm, porosity 10 – 20 µm). Then, 225 mg of $SnCl_2$ were dissolved in air in 5 ml of concentrated HCl (ACROS OrganicsTM, 37 wt. % solution in water). After full dissolution, the latter solution was added to the solution of **1**. Afterwards, this solution was slowly heated to 80°C in air under stirring. Heating was stopped after 45 min. A second acidic solution was added and the solution was let to cool down. When the temperature of 30°C was reached, a third acidic solution was added and the beaker was put in ice. Microcrystalline powder was recovered after filtration on a glass frit (1 – 1.6 µm). The powder was then washed with HCl and ether and dried over P_2O_5 at room temperature for 24 h; yield 0.77 g, 92.7 % subtracting **1** impurities. EDS analysis of heavy elements *i.e.* Cl and Nb for selected crystals from the preparation revealed an average atomic composition of 70 % for chorine and 30 % for niobium in full agreement with the theoretical one for Nb_6Cl_{14} (30:70).

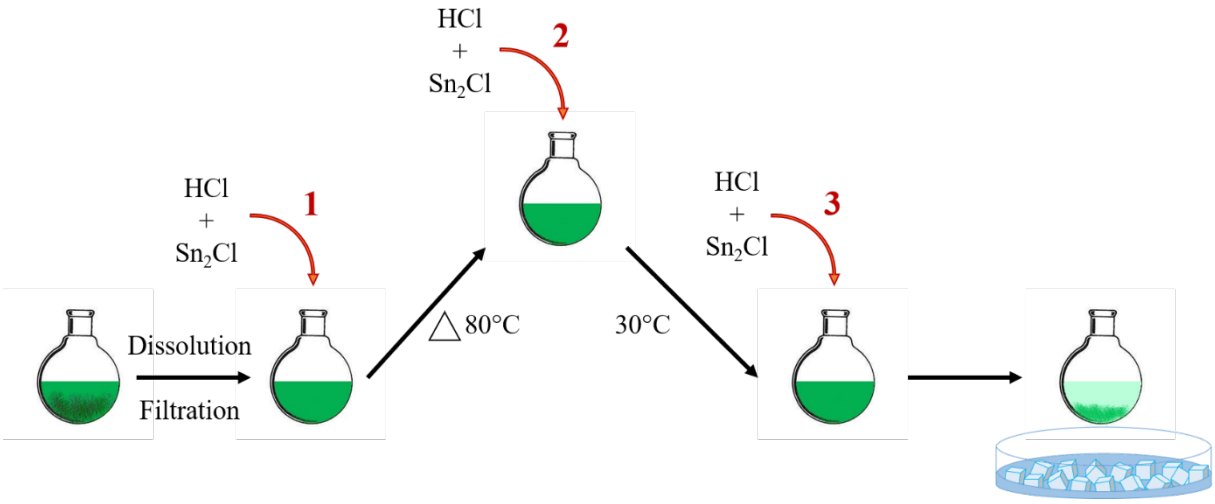

Scheme S2. Synthesis of $[\{Nb_6Cl^i_{12}\}Cl^a_2(H_2O)^a_4]\cdot 4H_2O$.

*Synthesis of (TBA)$_3$ [{Nb$_6$Cl$^i_{12}$}Cl$^a_6$] (**3**).* 200 mg of **1** were diluted in 20 mL of acetone and stirred for 24 hours under air. The resulting yellowish solution was filtered on a membrane filter (Sartorius, PTFE 0.2 µm) and 0.123 g (4.44 10^{-4} mol) of (TBA)Cl ($TBA^+ = [N(C_4H_9)_4]^+$) were added to the solution and leave stirred for 24 extra hours. The solvent was then evaporated and the powder was washed with ethanol in order to remove extra TBA salt without dissolving **3**. 5 mL of acetone were used to dissolve the powder and to extract **3**. 57.6 mg of single crystals were obtained by slow diffraction of ether; yield 28.8 % considering **1** as impurities. The single crystals were used as starting materials and they were dried 1 h in an oven at 60°C after recovering.

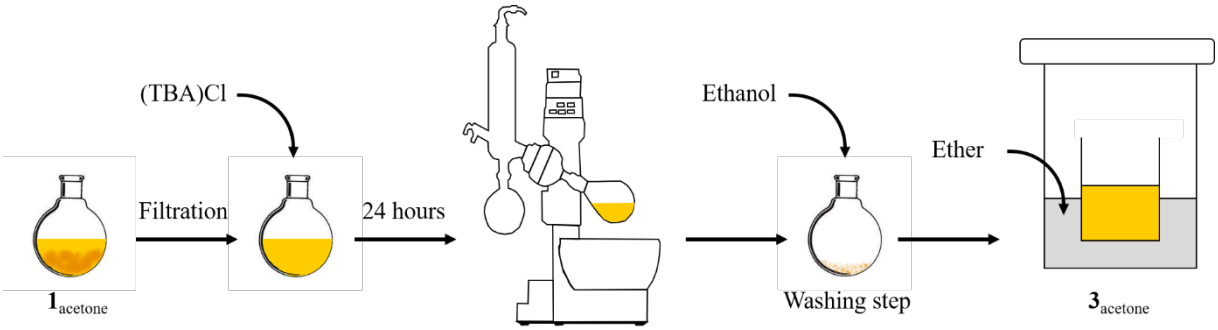

Scheme S3. Synthesis of $(TBA)_3[\{Nb_6Cl^i_{12}\}Cl^a_6]$.

*Preparation method of solutions of **1** for spectroscopic investigations.* Solutions of **1** were prepared as follows: 20 mg of **1** were dissolved per milliliter of solution (water or acetone), stirred overnight at 350 tr/min and then, filtered (on a filter paper, thickness 0.15 mm, porosity 10 – 20 µm) out to get rid of non-dissolved impurities. When acetone was used as solvent, the dissolution was carried out in dried acetone during 24 hours under argon using Schlenk techniques. The stirring was then stopped and the solution let to decantation. The solution appeared green-olive but turned spontaneously brown when

opening the Schlenk tube. When solubilizing **1** in acetone in atmospheric condition using the same protocol, a brown solution is obtained since the early stage of dissolution. The solutions obtained from **1** after filtration in water and acetone will be denoted $\mathbf{1}_{water}$ and $\mathbf{1}_{acetone}$ respectively.

Raman solid-state measurements. Raman scattering spectra from 1100 cm^{-1} to 100 cm^{-1} were acquired for **1** as powders, for $\mathbf{1_{water}}$ as solution and for **3** as single crystal at room temperature using a LabRamHigh resolution spectrometer coupled with a confocal microscope (Horiba Jobin Yvon), 600 g/mm gratings and 10 × or 100 × objective. A He-Ne 633 nm laser was used for scattering excitation. Raman spectra were recorded at room temperature with the 10 × objective at 10% power during 100 s exposition and 2 accumulations for **1**, the 10 × objective at 100% power during 50 s exposition and 2 accumulations for $\mathbf{1_{water}}$ and with the 100 × objective at 1% power during 60 s exposition and 2 accumulations for **3**. The calibration of the Raman spectrometer was performed using the main Raman band of silicon wafer (520 cm^{-1}).

Electrochemical solution measurements. The electrochemical characterization by cyclic voltammetry was performed at room temperature using a conventional three-electrode cell in the Nb_6-containing electrolytic solution. This solution consists of 1 mM of **3** in a solution of 0.1 M of tetrabutylammonium hexafluorophosphate (TBA)[PF_6] in dichloromethane (column chromatography purification). A glassy carbon electrode was used as working electrode, a platinum wire as counter-electrode, and an Ag/AgCl electrode as reference electrode. The solution was degassed by N_2 before performing the electrochemical measurements. Because cyclic voltammetry measurements were not done in closed system, it has to be mentioned that, even if limited, some solvent evaporation occurs leading to slight changes in the solution concentration. The cyclic voltammetry scans were recorded in a potential window of -0.40 V to 0.70 V versus Ag/AgCl at 0.1 $V.s^{-1}$ using a Metrohm Autolab PGSTAT30. Both negative and positive potentials were applied from the initial equilibrium potential (0.15 V vs Ag/AgCl) leading to anodic currents and cathodic currents respectively.

The two reversible one-electron transfer processes of niobium chloride octahedral cluster have been reported in different media, using specific cluster compounds[2–6], and gathered in Table S1.

Table S1. Summary of electrochemical measurements of $\{Nb_6Cl^i_{12}\}^{2+}$ cluster units reported in the literature and made in this work

Initial cluster compound	Reference	Redox system	$E_{1/2}$, V (vs Ag/AgCl and for comparison vs ferrocenium/ferrocene in brackets)	Solvent

$[\{Nb_6Cl^i_{12}\}Cl^a_2(H_2O)^a_4].4\ H_2O$	[4]	$\{Nb_6Cl^i_{12}\}^{2+/3+}$	0.58 (0.988)	2M $HClO_4$
$[\{Nb_6Cl^i_{12}\}Cl^a_2(H_2O)^a_4].4\ H_2O$	[5]	$\{Nb_6Cl^i_{12}\}^{2+/3+}$	0.58 (0.988)	H_2O
$[\{Nb_6Cl^i_{12}\}Cl^a_2(H_2O)^a_4].4\ H_2O$	[5]	$\{Nb_6Cl^i_{12}\}^{3+/4+}$	0.87 (1.278)	H_2O
*$[MeEtim]_2[\{Nb_6Cl^i_{12}\}Cl^a_6]$	[6]	$\{Nb_6Cl^i_{12}\}^{2+/3+}$	-0.020 (0.388)	$AlCl_3$ (44.4 mol %) – MeEtim
$[MeEtim]_2[\{Nb_6Cl^i_{12}\}Cl^a_6]$	[6]	$\{Nb_6Cl^i_{12}\}^{3+/4+}$	0.391 (0.799)	$AlCl_3$ (44.4 mol %) – MeEtim
**$[TEA]_3[\{Nb_6Cl^i_{12}\}Cl^a_6]$	[7]	$\{Nb_6Cl^i_{12}\}^{2+/3+}$	-0.17[b] (0.437)	CH_3CN
$[TEA]_3[\{Nb_6Cl^i_{12}\}Cl^a_6]$	[7]	$\{Nb_6Cl^i_{12}\}^{3+/4+}$	0.39[b] (0.756)	CH_3CN
***$[TBA]_3[\{Nb_6Cl^i_{12}\}Cl^a_6]$	[8]	$\{Nb_6Cl^i_{12}\}^{2+/3+}$	-0.205 (0.203)	$CHCl_2$
$[TBA]_3[\{Nb_6Cl^i_{12}\}Cl^a_6]$	[8]	$\{Nb_6Cl^i_{12}\}^{3+/4+}$	0.330 (0.738)	$CHCl_2$
$[TBA]_3[\{Nb_6Cl^i_{12}\}Cl^a_6]$	This work	$\{Nb_6Cl^i_{12}\}^{2+/3+}$	-0.20 (0.208)	$CHCl_2$
$[TBA]_3[\{Nb_6Cl^i_{12}\}Cl^a_6]$	This work	$\{Nb_6Cl^i_{12}\}^{3+/4+}$	0.33 (0.738)	$CHCl_2$

*$[MeEtim]^+$ = 1-Methyl-3-ethylimidazolium **$[TEA]^+ = [N(C_2H_5)_4]^+$ ***$[TBA]^+ = [N(C_4H_9)_4]^+$

[a] $E_{1/2}$, V (vs SHE)

[b] $E_{1/2}$, V (vs SCE)

Concerning this work, measurements have been done in DCM in order to avoid solvent coordination and apical exchanges. Both anodic (from positive to negative potentials) and cathodic sweep (from negative to positive potentials) have been recorded (Figure S2). In both cases, two reversible one-electron transfer could be observed around -0.20 V vs Ag/AgCl ($E_{1,ox}$ = -0.15 V vs Ag/AgCl, $E_{1,red}$ = -0.25 V vs Ag/AgCl) for the reversible reduction of a $\{Nb_6Cl^i_{12}\}^{3+}$-core species to a $\{Nb_6Cl^i_{12}\}^{2+}$-core species (Eq. 1) and around 0.33 V vs Ag/AgCl ($E_{1,ox}$ = 0.38 V vs Ag/AgCl, $E_{1,red}$ = 0.27 V vs Ag/AgCl) for the reversible oxidation of a $\{Nb_6Cl^i_{12}\}^{3+}$-core species to a $\{Nb_6Cl_{i12}\}^{4+}$-core species (Eq. 2).

$$\{Nb_6Cl^i_{12}\}^{3+} + e^- \rightarrow \{Nb_6Cl^i_{12}\}^{2+} \qquad \text{Eq. 1}$$

$$\{Nb_6Cl^i_{12}\}^{4+} + e^- \rightarrow \{Nb_6Cl^i_{12}\}^{3+} \qquad \text{Eq. 2}$$

Potential values measured in DCM are identical as those reported by Prokopuk *et al.*[9] but noticeably different from those measured in water.[5,6] Indeed, an oxidation potential negative shift of around 0.6 V is observed between acidic aqueous media and DCM. Such shift is generally stated when experiments are done in aqueous and organic media, but the change of media alone is not enough to explain that large shift. The exchange of apical ligands, from $[\{Nb_6Cl^i_{12}\}Cl^a_6]^{n-}$ to $[\{Nb_6Cl^i_{12}\}(H_2O)^a_6]^{n+}$, in aqueous solution is another origin of the shift.

UV-vis spectrometry. Absorption spectra of the solutions and transmission spectra of the films were evaluated by a high-performance UV/VIS/NIR spectrophotometer (V770, Jasco) with an integrated sphere, in the 250 nm – 2500 nm range.

Mass Spectrometry. Mass spectrometry (ESI-MS) measurements with ionization by electrospray or nanospray source were recorded on a quadrupole time-of-flight mass spectrometer (microtof-Q, Bruker-Daltonics, Bremen, Germany). The samples $\mathbf{1}_{\mathbf{water}}$ and $\mathbf{1}_{\mathbf{acetone}}$ were analyzed both in negative and positive ion mode. Each solution sample was prepared to approximately reach 50 µmol.L^{-1} (residual impurities preventing to reach a completely quantitative concentration) in appropriate solvent, *i.e.*, water or acetone. The water solution was infused directly in an electrospray source using a syringe pump (flow rate 180 µL.h^{-1}) and the ESI process was assisted with a dry gas at 80°C. The acetone solution was infused directly in a nanospray source with dry gas temperature set at 55°C.

Powder X-ray diffraction experiments. X-ray powder diffraction (XRPD) data were recorded at room temperature using a Bruker D8 Advance two-circle diffractometer (θ−2θ Bragg-Brentano mode) using Cu Kα radiation (λ = 1.54056 Å) equipped with a Ge(111) monochromator and a Lynx Eye detector. The analyses of the diffraction patterns were performed by profile refinement using the FullProf and WinPlotr software packages.[10,11]

Measurement of haze and clarity values. The measurement of haze was carried out following the Standard Test Method "ASTM D-1003". A HazeGard Plus hazemeter apparatus from '*OAKLAND Instrument Corporation*' was used to measure simultaneously the haze, transmission and clarity values.

Films preparation. PVP films were obtained by drop-casting from aqueous solution of **1** ($\mathbf{1}_{\mathbf{water}}$) and ($\mathbf{2}_{\mathbf{water}}$) and from a dichloromethane solution of **3** ($\mathbf{3}_{\mathbf{DCM}}$). As depicted in Scheme 1, after dissolution of **1** in water (from 2.0 to 20.0 g.L^{-1} of $K_4[\{Ta_6Br^i_{12}\}Br^a_6]$), $\mathbf{1}_{\mathbf{water}}$ was filtered (filter paper, thickness 0.15 mm, porosity 10 – 20 µm) to eliminate niobium metal impurities. $\mathbf{2}_{\mathbf{water}}$ (1.25 to 12.5 g.L^{-1}) or $\mathbf{3}_{\mathbf{DCM}}$ (1.10^{-3} mol.L^{-1}) solutions were used without filtration for the films' preparation. PVP (Sigma- Aldrich M = 1 300 000 g.mol^{-1}) is solid at room temperature. It was added at 10% weight ratio to $\mathbf{1}_{\mathbf{water}}$, $\mathbf{2}_{\mathbf{water}}$ or $\mathbf{3}_{\mathbf{DCM}}$ and stirred until homogenization (1 – 2 hours). PVP-based solutions are stable over months. They were drop-coated homogeneously in order to cover glass substrates (1 mL for a 7.5 × 2.5 cm substrate). The films were let gently solidify by evaporation of the solvent in few hours (6 for water and 1 for dichloromethane). This latter step was made at room temperature under atmosphere condition.

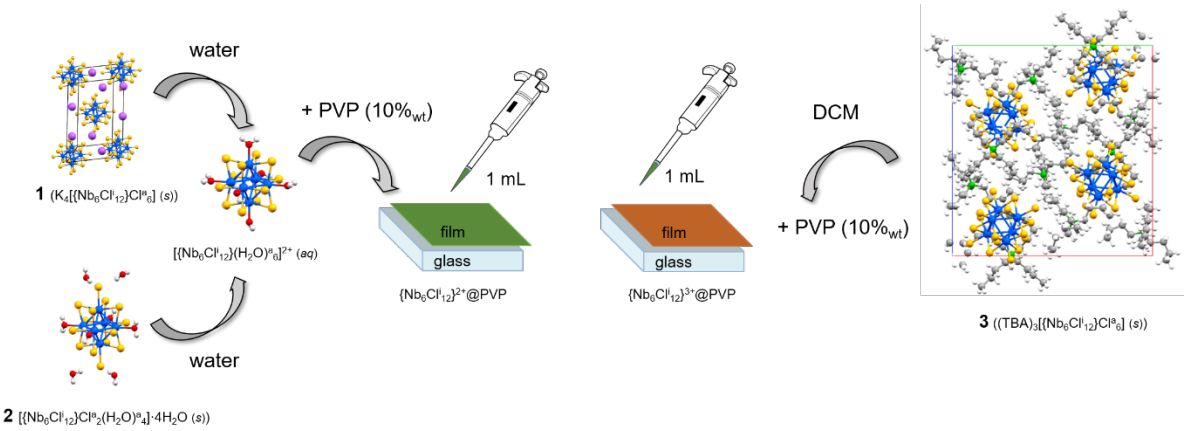

Scheme S4. Film preparation from **1**, **2** and **3** solutions.

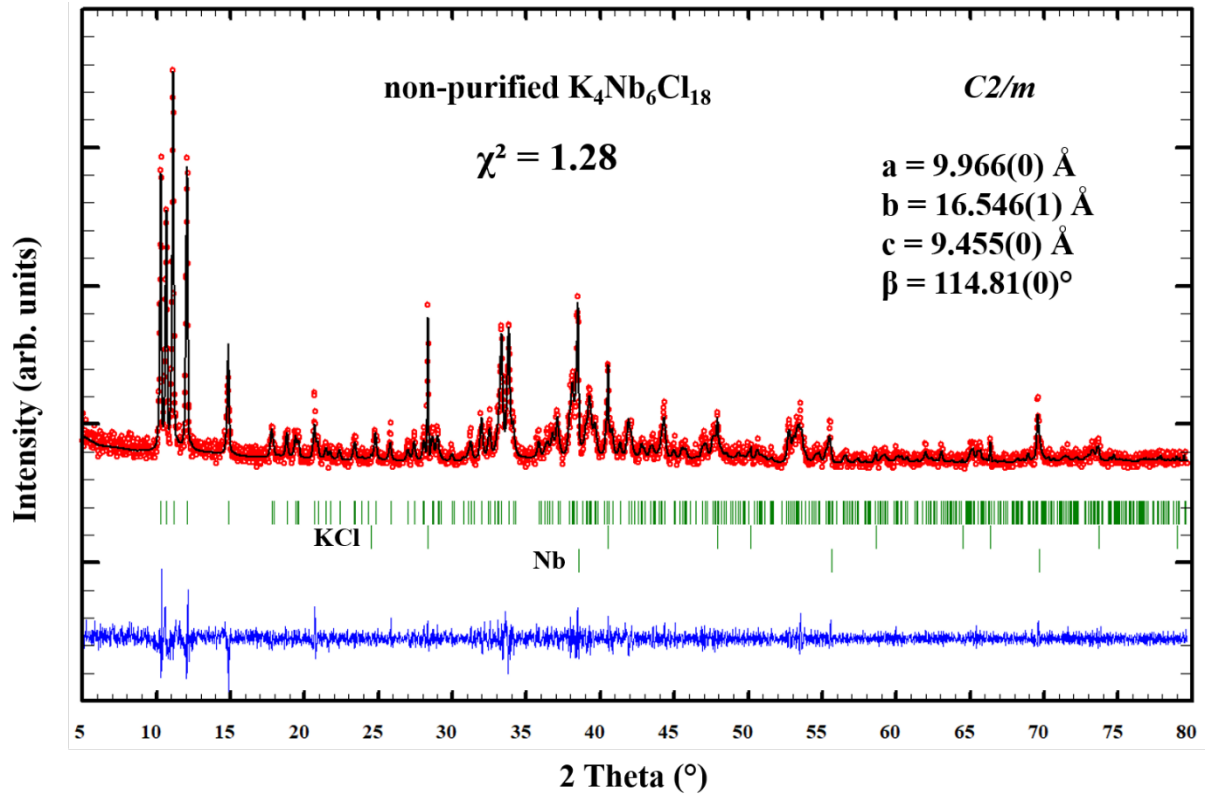

Figure S1. Le Bail refinement of the XRPD pattern of the crude powder containing **1** recorded at room temperature.

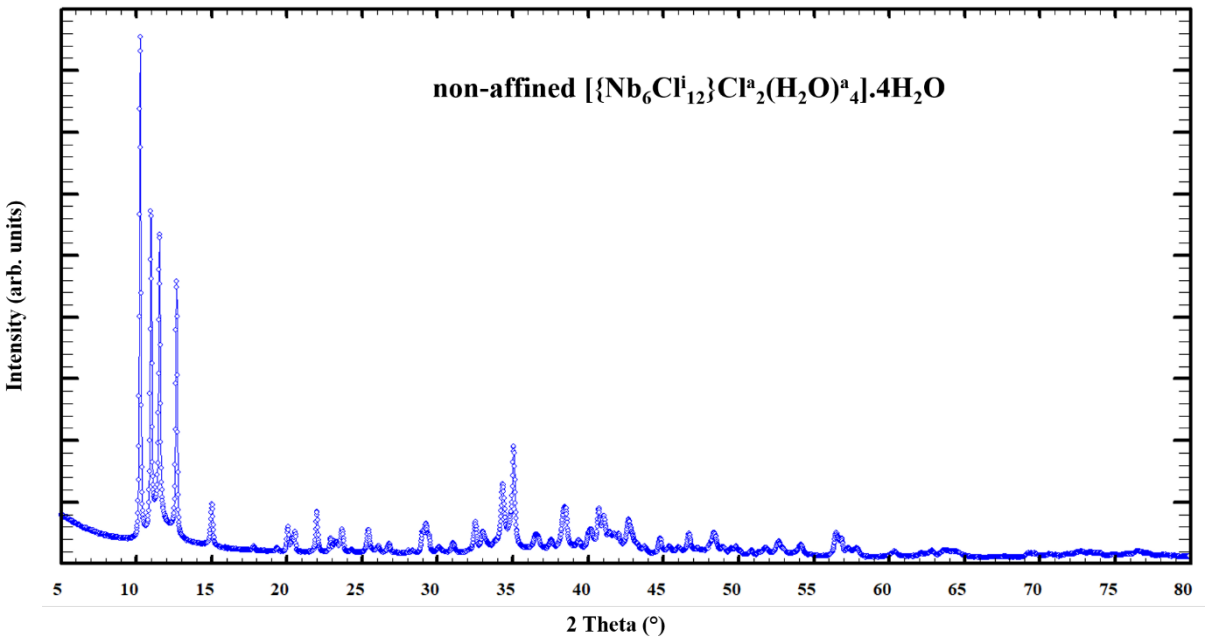

Figure S2. Raw data of the XRPD pattern of the powder of **2** recorded at room temperature.

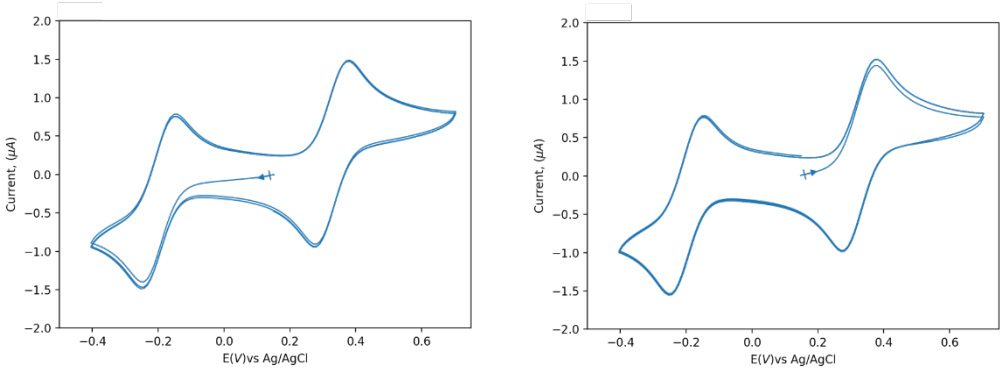

Figure S3. Cyclic voltammograms of 1.10^{-3} M of **3** in DCM (1.10^{-1} M of (TBA)[PF_6]) recorded starting by applying an anodic sweep (left) or cathodic sweep (right).

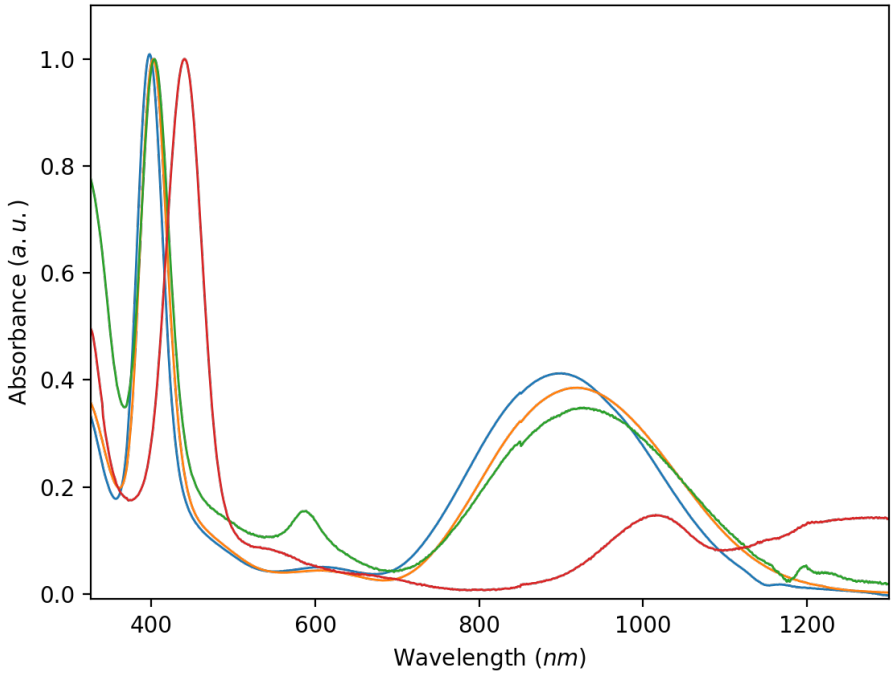

Figure S4. Normalized UV-visible absorption spectra of solution **1** at RT in water (blue spectrum), methanol (orange spectrum), ethanol (green spectrum), and acetone (red spectrum).

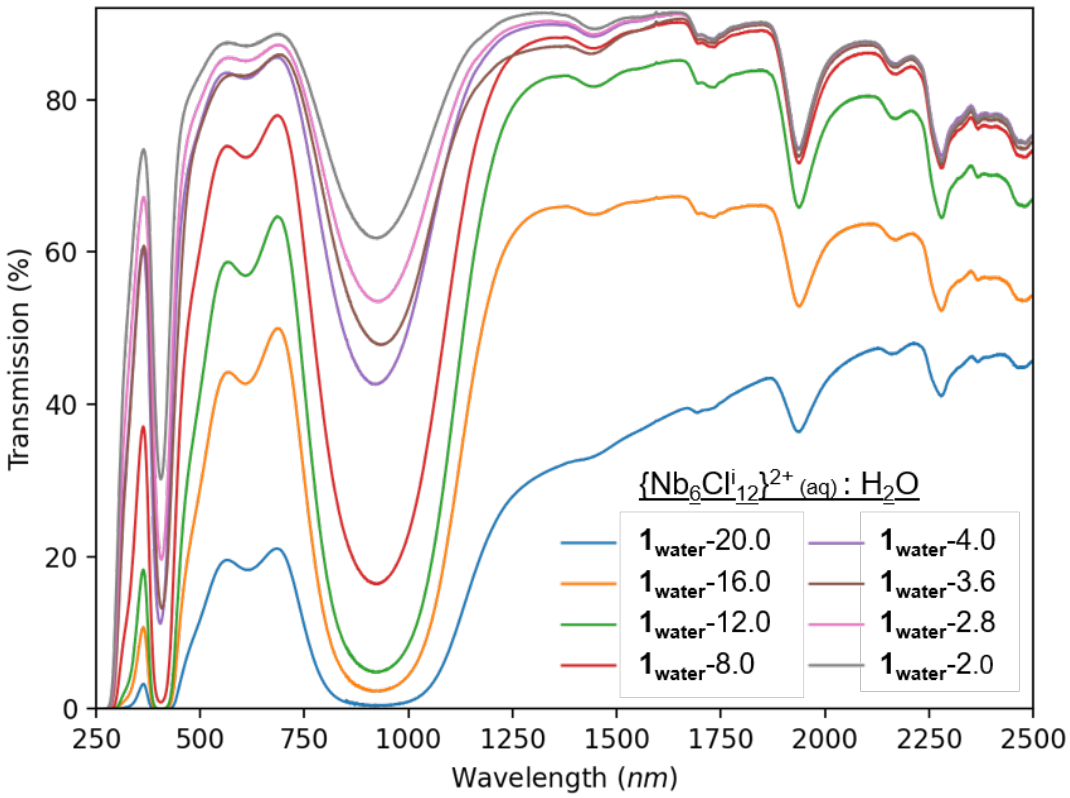

Figure S5. UV-visible transmission spectra of $\{Nb_6Cl^i_{12}\}^{2+}$ cluster unit in PVP film, 1 month after coating on glass substrate.

Table S2. x, y and z color coordinates and the FOM values of $\{Nb_6Cl^i_{12}\}^{2+}$ cluster unit in PVP film, 1-month after coating on glass substrate.

	x	y	z	T_{vis}	T_{sol}	T_{vis}/T_{sol}
$\{Nb_6Cl^i_{12}\}^{2+}$(aq) : H_2O	***1-month aging***					
1$_{water}$-20.0	0.417	0.464	0.119	17.3	14.2	1.2
1$_{water}$-16.0	0.406	0.449	0.145	40.0	31.2	1.3
1$_{water}$-12.0	0.395	0.439	0.166	53.9	42.1	1.3
1$_{water}$-8.0	0.369	0.413	0.217	70.1	55.7	1.3
1$_{water}$-4.0	0.342	0.376	0.282	81.5	70.4	1.2
1$_{water}$-3.6	0.349	0.386	0.264	81.0	70.9	1.1
1$_{water}$-2.8	0.338	0.370	0.292	83.8	74.7	1.1
1$_{water}$-2.0	0.330	0.358	0.312	86.2	78.8	1.1

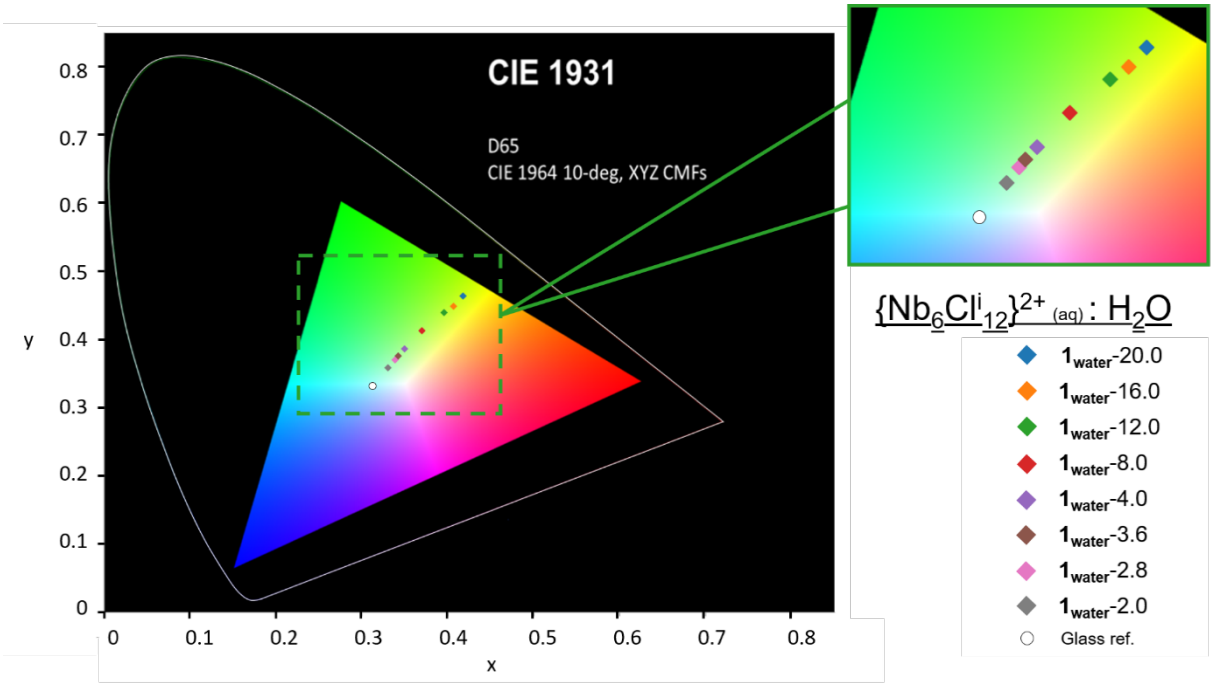

Figure S6. CIE chromaticity coordinates of $\{Nb_6Cl^i_{12}\}^{2+}$ cluster unit in PVP film, 1 month after coating on glass substrate.

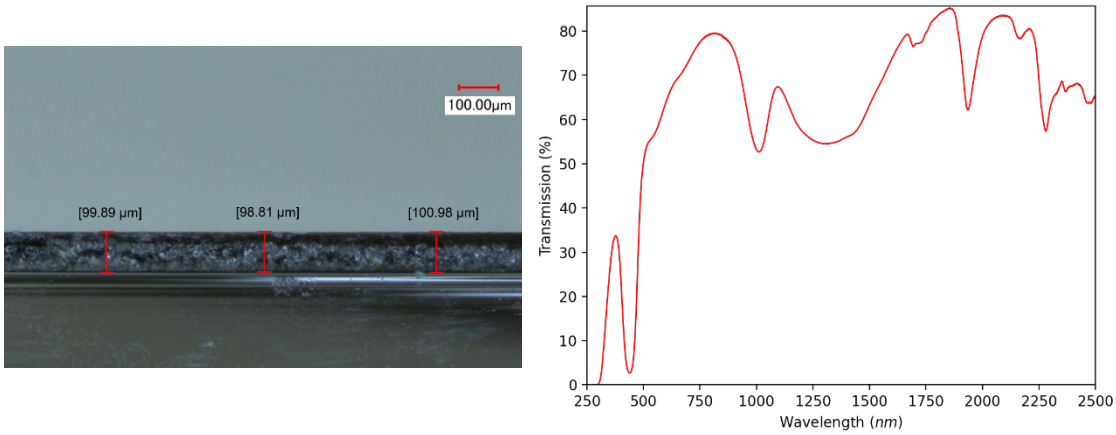

Figure S7. Digital microscopy image of the cross section of a $\{Nb_6Cl^i_{12}\}^{3+}$@DCM@PVP film (left). UV-visible transmission spectra of a film of $\{Nb_6Cl^i_{12}\}^{3+}$@DCM@PVP film (right).

Table S3. x, y and z color coordinates and the FOM values of $\{Nb_6Cl^i_{12}\}^{3+}$ cluster unit in PVP film, coated on glass substrate.

	x	y	z	T_{vis}	T_{sol}	T_{vis}/T_{sol}
$\{Nb_6Cl^i_{12}\}^{3+}$ @DCM@PVP	0.417	0.464	0.119	57.07	58.25	0.98

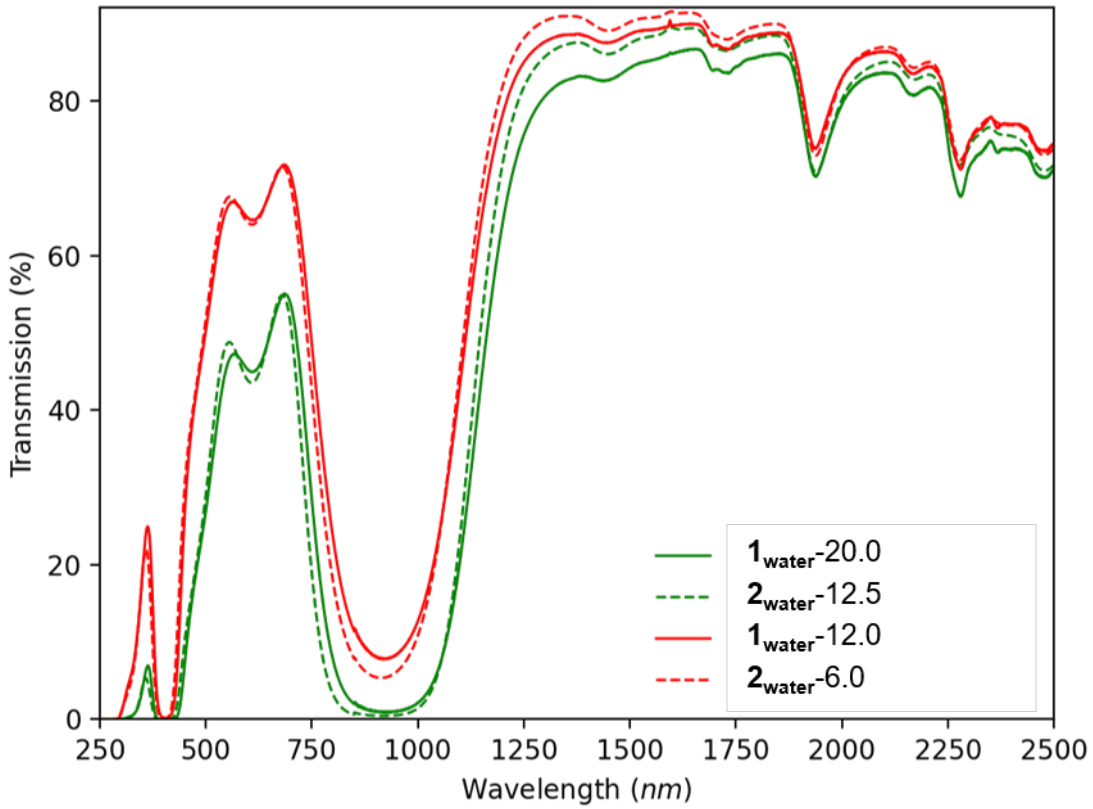

Figure S8. UV-visible transmission spectra of $\{Nb_6Cl^i_{12}\}^{2+}$ cluster unit in PVP film, coated on glass substrate.

Table S4. CIE x, y and z color coordinates and the FOM values of $\{Nb_6Cl^i_{12}\}^{2+}$ cluster unit embedded in PVP film and coated on glass substrate, starting from $\mathbf{1}_{water}$ and $\mathbf{2}_{water}$ solutions.

	x	y	z	T_{vis}	T_{sol}	T_{vis}/T_{sol}
$\{Nb_6Cl^i_{12}\}^{2+}(aq) : H_2O$						
$\mathbf{1}_{water}$-20.0	0.423	0.463	0.113	41.5	33.8	1.2
$\mathbf{1}_{water}$-12.0	0.382	0.427	0.190	62.2	48.3	1.3
$\mathbf{2}_{water}$-12.5	0.422	0.466	0.112	41.6	33.4	1.2
$\mathbf{2}_{water}$-6.0	0.375	0.421	0.204	63.0	47.9	1.3

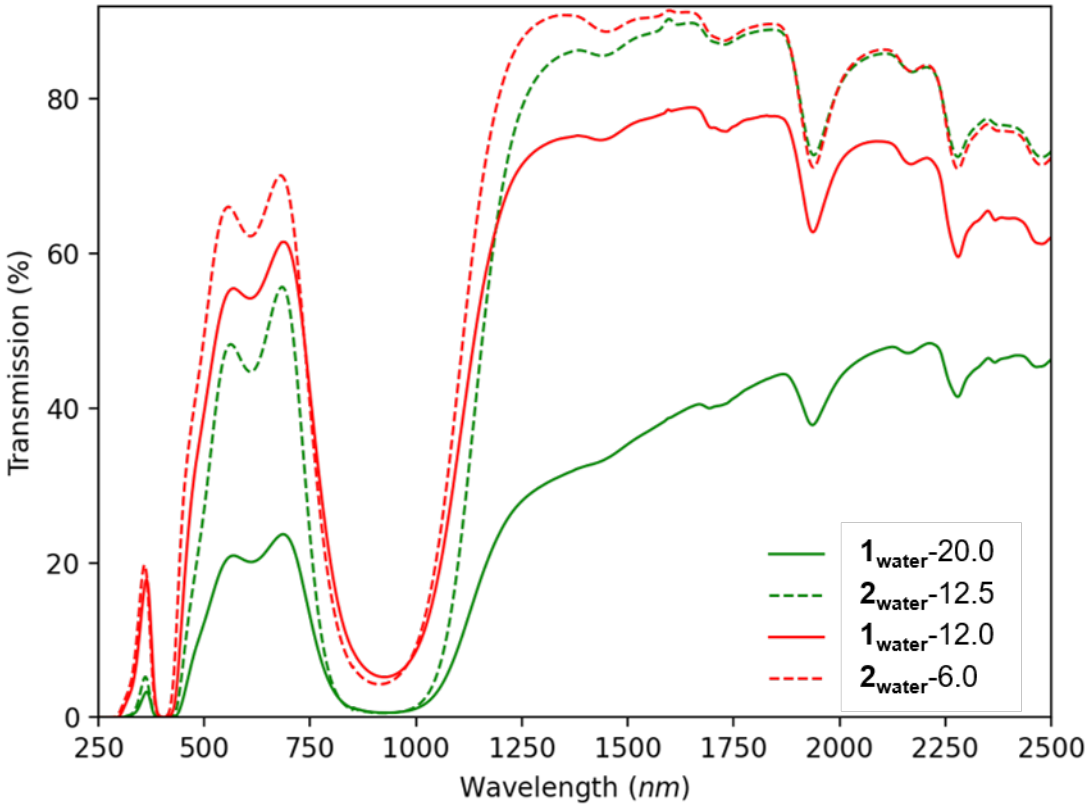

Figure S9. UV-visible transmission spectra of aged $\{Nb_6Cl^i_{12}\}^{2+}$ cluster unit in PVP film, coated on glass substrate.

Table S5. CIE x, y and z color coordinates and the FOM values of one-month aged $\{Nb_6Cl^i_{12}\}^{2+}$ cluster unit embedded in PVP film and coated on glass substrate, starting from $\mathbf{1}_{water}$ and $\mathbf{2}_{water}$ solutions.

	x	y	z	T_{vis}	T_{sol}	T_{vis}/T_{sol}
$\{Nb_6Cl^i_{12}\}^{2+}(aq) : H_2O$						
$\mathbf{1}_{water}$-20.0	0.417	0.464	0.119	17.3	14.2	1.2
$\mathbf{1}_{water}$-12.0	0.395	0.439	0.166	53.9	42.1	1.3
$\mathbf{2}_{water}$-12.5	0.422	0.466	0.112	42.3	33.9	1.2
$\mathbf{2}_{water}$-6.0	0.378	0.424	0.196	61.2	46.4	1.3

Table S6. T_{vis}, haze and clarity value of clusters@PVP films 24 h after their preparation.

	T_{vis}	Haze	Clarity
Sample			
Glass sample	92.8	1.02	99.7
$\mathbf{1}_{water}$-16.0	56.0	22.6	91.8
$\mathbf{1}_{water}$-12.0	61.5	12.2	92.0
$\mathbf{1}_{water}$-8.0	71.1	5.91	94.0
$\mathbf{1}_{water}$-3.6	82.9	1.44	98.0
$\mathbf{1}_{water}$-2.0	87.4	1.49	99.2
$\mathbf{2}_{water}$-12.5	44.3	1.30	99.2
$\mathbf{2}_{water}$-7.5	54.0	1.06	98.6
$\mathbf{2}_{water}$-6.0	60.5	1.44	99.4

The NIR shielding value (S_{NIR}) is calculated as follow:

$S_{NIR}(\%) = 100 - \frac{\int_{760}^{2500} T(\lambda)S(\lambda)d\lambda}{\int_{760}^{2500} S(\lambda)d\lambda}$ where:

- T is the transmission spectrum.
- S represents the Air Mass 1.5 (AM 1.5), which is equivalent to the spectrum of solar radiation after passing through 1.5 times the perpendicular atmospheric thickness

Table S7. NIR shielding values of clusters@PVP films 24 h and one-month in ambient conditions after their preparation.

24-hours after preparation		1-month after preparation	
	S_{NIR} (%)		S_{NIR} (%)
Glass substrate	8.3		
$\mathbf{1}_{water}$-20.0	63.9	$\mathbf{1}_{water}$-20.0	83.7
$\mathbf{1}_{water}$-16.0	61.7	$\mathbf{1}_{water}$-16.0	70.6
$\mathbf{1}_{water}$-12.0	53.7	$\mathbf{1}_{water}$-12.0	61.4
$\mathbf{1}_{water}$-8.0	45.1	$\mathbf{1}_{water}$-8.0	49.1
$\mathbf{1}_{water}$-4.0	31.8	$\mathbf{1}_{water}$-4.0	35.3
$\mathbf{1}_{water}$-3.6	30.1	$\mathbf{1}_{water}$-3.6	34.3
$\mathbf{1}_{water}$-2.8	26.9	$\mathbf{1}_{water}$-2.8	26.4
$\mathbf{1}_{water}$-2.0	22.6	$\mathbf{1}_{water}$-2.0	22.4
$\mathbf{2}_{water}$-12.5	63.4	$\mathbf{2}_{water}$-12.5	63.2
$\mathbf{2}_{water}$-6.0	54.3	$\mathbf{2}_{water}$-6.0	55.4
$\{Nb_6Cl^i_{12}\}^{3+}$@DCM@PVP	32.0		

II. Computational study

Computational details

Molecular density functional (DFT) calculations were carried out using the Amsterdam Density Functional (ADF 2019) program package developed by Baerend *et. al.*[12,13] The local density approximation description[14] was corrected thanks to the revPBE exchange and correlation nonlocal gradient.[15] Relativistic effects were treated at the first-order of perturbation using a ZORA Hamiltonian.[16,17] The all-electron ADF QZ4P Slater-type atomic basis set has been used, *i.e.* a quadruple-ζ STO basis set completed with four polarization functions. This protocol was successfully employed to study ground states and optical properties of $[\{Mo_6Br^i_8\}L^a_6]^{2-}$ and $[\{Ta_6Br^i_{12}\}L_6]^{n-}$ metal cluster in good agreement with experimental results.[18,19] No symmetry constraint was used during the geometry optimization but if the final geometry was presenting symmetry elements (variation distances < 0.001 Å), the symmetry was later imposed and validated by checking the total energy. The local minimum character of every system was checked via vibrational frequency calculations. Spectroscopic properties (IR, UV-Vis and Raman (laser frequency 1.958 eV/ 633 nm)) were simulated using the modules provided in ADF Modeling suite. Table S3 gathers the Cartesian coordinates of the optimized structures.

Table S8. Cartesian coordinates of the optimized geometries $[\{Nb_6Cl^i_{12}\}Cl^a_6]^{4-}$ (n = 2-4), $[\{Nb_6Cl^i_{12}\}(H_2O)^a_4]^{2+}$, $[\{Nb_6Cl^i_{12}\}(H_2O)^a_6]^{2+}$, $[\{Nb_6Cl^i_{12}\}(OH)^a_6]^{n-}$ (n = 2 or 4), $[\{Nb_6Cl^i_{12}\}$*trans*-$Cl^a_2(H_2O)^a_4]$, $[\{Nb_6Cl^i_{12}\}(OH)^a_1(OH_2)^a_5]$ and $[\{Nb_6Cl^i_{12}\}$*trans*-$(OH)^a_2(OH_2)^a_4]$.

$[\{Nb_6Cl^i_{12}\}Cl^a_6]^{4-}$

Nb	-0.000071	-2.109654	-0.000068
Nb	0.000007	0.000053	-2.109699
Nb	0.000074	2.109676	0.000045
Nb	-0.000005	-0.000062	2.109722
Nb	-2.109796	0.000071	-0.000003
Nb	2.109797	-0.000075	0.000011
Cl	2.468628	-0.000002	-2.468602
Cl	-0.000153	-4.820765	-0.000175
Cl	0.000094	2.468667	-2.468533
Cl	-0.000007	-0.000196	4.820804
Cl	2.468534	-2.468682	-0.000080
Cl	0.000153	4.820772	0.000157
Cl	-2.468627	-0.000002	2.468609
Cl	-2.468704	-2.468514	-0.000089
Cl	-0.000077	-2.468525	-2.468676
Cl	0.000073	2.468513	2.468678
Cl	2.468695	2.468526	0.000091
Cl	-0.000008	0.000146	-4.820790
Cl	-4.820861	0.000194	-0.000026
Cl	2.468606	-0.000167	2.468621
Cl	-0.000090	-2.468682	2.468506
Cl	-2.468606	0.000164	-2.468606
Cl	-2.468519	2.468691	0.000073
Cl	4.820862	-0.000145	0.000031

$[\{Nb_6Cl^i_{12}\}Cl^a_6]^{3-}$

Nb	-0.003345	-2.143665	-0.003481
Nb	-0.000109	0.003479	-2.143692
Nb	0.003346	2.143676	0.003468
Nb	0.000111	-0.003469	2.143704
Nb	-2.143734	0.003336	0.000123
Nb	2.143734	-0.003353	-0.000120
Cl	2.457182	0.000160	-2.457441
Cl	-0.007330	-4.748015	-0.007643
Cl	0.003810	2.461298	-2.453300
Cl	0.000251	-0.007646	4.748049
Cl	2.453457	-2.461146	-0.004244
Cl	0.007331	4.748022	0.007631
Cl	-2.457180	-0.000162	2.457445
Cl	-2.461156	-2.453451	-0.003960
Cl	-0.004076	-2.453287	-2.461303
Cl	0.004072	2.453293	2.461301
Cl	2.461154	2.453446	0.003964
Cl	-0.000254	0.007637	-4.748041
Cl	-4.748074	0.007342	0.000258
Cl	2.457432	-0.008046	2.457166
Cl	-0.003809	-2.461295	2.453287
Cl	-2.457433	0.008044	-2.457159
Cl	-2.453452	2.461141	0.004242
Cl	4.748074	-0.007338	-0.000252

$[\{Nb_6Cl^i_{12}\}Cl^a_6]^{2-}$

Nb	-0.053425	-2.174534	-0.060039
Nb	-0.000795	0.060003	-2.175017
Nb	0.053425	2.174532	0.060041

Nb	0.000795	-0.060001	2.175014
Nb	-2.175121	0.053237	0.002940
Nb	2.175121	-0.053236	-0.002940
Cl	2.445391	0.007572	-2.449391
Cl	-0.116269	-4.701221	-0.130684
Cl	0.059116	2.512875	-2.378845
Cl	0.002001	-0.130769	4.702734
Cl	2.386459	-2.505289	-0.070824
Cl	0.116269	4.701219	0.130684
Cl	-2.445391	-0.007575	2.449390
Cl	-2.506345	-2.385763	-0.065334
Cl	-0.062074	-2.378187	-2.513588
Cl	0.062073	2.378191	2.513585
Cl	2.506348	2.385760	0.065336
Cl	-0.002005	0.130785	-4.702734
Cl	-4.703105	0.116086	0.006119
Cl	2.447371	-0.128517	2.443006
Cl	-0.059112	-2.512873	2.378850
Cl	-2.447371	0.128516	-2.443007
Cl	-2.386462	2.505288	0.070822
Cl	4.703103	-0.116098	-0.006116

$[\{Nb_6Cl^i_{12}\}(H_2O)^a_4]^{2+}$

Nb	0.044137	-2.058490	0.076253
Nb	-0.031785	-0.012003	2.157311
Nb	-2.000783	-0.028451	0.057233
Nb	0.026863	0.024527	-1.978807
Nb	-0.039338	2.077338	0.111277
Nb	2.000443	0.051299	0.113118
Cl	0.015709	-2.470388	2.528633
Cl	-0.084303	2.420612	2.575110
Cl	-2.423322	-2.454866	0.032763
Cl	2.527153	-2.344681	0.102240
Cl	-2.513281	-0.060334	2.455192
Cl	-2.438685	-0.019424	-2.375280
Cl	2.498364	0.078180	-2.308414
Cl	-2.514143	2.389807	0.073974
Cl	-0.016080	2.477387	-2.327614
Cl	0.082067	-2.435112	-2.371734
Cl	2.424389	2.484110	0.142174
Cl	2.438473	0.038131	2.536000
H	-0.087797	-4.938340	-0.703308
H	0.699524	4.950551	-0.100731
H	0.009033	0.768491	5.027745
H	0.812827	-0.219209	-4.851526
O	-0.129322	-0.038098	4.502620
H	0.212721	-0.776254	5.034702
O	-0.063631	4.428690	0.201041
H	-0.855588	4.939903	-0.038091
O	0.054325	0.094892	-4.330725
H	-0.739668	-0.093421	-4.859434
O	0.158921	-4.405565	0.071552
H	-0.065046	-4.936852	0.854378

$[\{Nb_6Cl^i_{12}\}(H_2O)^a_6]^{2+}$

Nb	0.039482	-2.051973	0.073954
Nb	-0.016402	-0.012537	2.142093
Nb	-2.057086	-0.025051	0.070823
Nb	0.012222	0.028825	-1.963239
Nb	2.057601	0.049959	0.097078
Nb	-0.033685	2.073064	0.115073
Cl	0.028744	-2.473074	2.529769
Cl	-0.057620	2.421093	2.580897
Cl	-2.396720	-2.484801	0.050404
Cl	2.498612	-2.386924	0.081271
Cl	-2.481604	-0.056612	2.505013
Cl	-2.443040	-0.008561	-2.390514
Cl	2.469400	0.074091	-2.359622
Cl	-2.488708	2.432214	0.095274
Cl	-0.027266	2.484266	-2.325463
Cl	0.058203	-2.431347	-2.378646
Cl	2.400174	2.515964	0.129535
Cl	2.445603	0.029238	2.548843
H	0.105123	0.770322	5.015436
H	-4.935523	0.244127	-0.696929
H	4.930225	-0.101143	0.880472
H	0.770567	-0.264857	-4.841459
H	-0.234332	-4.926839	-0.680506
H	0.754898	4.936469	0.013974
O	-0.106723	-0.033892	4.511951
H	0.246857	-0.779123	5.025950
O	4.431073	0.157828	0.087235
H	4.924769	-0.201386	-0.669569
O	-0.060499	4.445535	0.213499
H	-0.784874	4.948518	-0.195620
O	0.029281	0.111124	-4.337402
H	-0.775034	-0.099312	-4.841294
O	-4.429127	-0.124936	0.046200
H	-4.931431	0.090664	0.850291
O	0.145769	-4.427701	0.062287
H	-0.089516	-4.922412	0.865707

$[\{Nb_6Cl^i_{12}\}(OH)^a_6]^{4-}$

Nb	-0.016963	-2.136263	0.137209
Nb	-0.168415	0.041036	2.199099
Nb	-2.126558	0.032837	-0.098746
Nb	0.170513	-0.055111	-2.029827
Nb	0.018769	2.152906	0.044250
Nb	2.131587	0.012732	0.252469
Cl	-0.213275	-2.469033	2.651378
Cl	-0.188747	2.555024	2.578111
Cl	-2.527462	-2.468281	-0.024916
Cl	2.482630	-2.497571	0.347210
Cl	-2.743252	0.095934	2.365910
Cl	-2.305218	-0.050915	-2.636969
Cl	2.714836	-0.054746	-2.224050
Cl	-2.476018	2.584897	-0.160633
Cl	0.187113	2.447322	-2.464938
Cl	0.151006	-2.584697	-2.332334
Cl	2.498378	2.529887	0.208565
Cl	2.313021	0.075251	2.764289
H	-0.221684	0.934788	4.610161
O	-0.347866	0.010705	4.342180
O	4.274534	0.019113	0.463812
H	4.606910	0.072436	-0.446083
O	0.089485	4.302422	0.021799
H	-0.828583	4.573890	-0.136451
O	0.401560	-0.124290	-4.169909
H	-0.480061	-0.357599	-4.501064
O	-4.262813	0.070333	-0.346329
H	-4.611623	0.031652	0.558631
O	-0.028825	-4.290079	0.144556
H	-0.022858	-4.529524	1.084663

$[\{Nb_6Cl^i_{12}\}(OH)^a_6]^{2-}$

Nb	0.042849	-2.186791	0.233544
Nb	-0.087435	0.119550	2.252732
Nb	-2.188944	-0.031618	-0.015703
Nb	0.078515	-0.141640	-2.079478
Nb	-0.053893	2.207240	-0.039856
Nb	2.179094	0.086998	0.160145
Cl	-0.040473	-2.340393	2.714404
Cl	-0.179390	2.601751	2.443425
Cl	-2.429673	-2.499874	0.193002
Cl	2.522411	-2.379002	0.332124
Cl	-2.606998	0.125332	2.430928
Cl	-2.377483	-0.217843	-2.499270
Cl	2.574339	-0.072007	-2.292675
Cl	-2.525321	2.464805	-0.131985
Cl	-0.011375	2.315007	-2.521755
Cl	0.117622	-2.636355	-2.201501
Cl	2.392703	2.569680	-0.004619
Cl	2.373452	0.253320	2.627625
H	-0.093207	1.036439	4.675992
O	-0.179374	0.135041	4.328879
O	4.248875	0.156176	0.310469
H	4.662300	0.212748	-0.564550
O	-0.018809	4.279943	-0.145090
H	-0.911421	4.642762	-0.254000
O	0.256468	-0.274259	-4.146121
H	-0.584355	-0.532258	-4.554023

O	-4.257424	-0.069054	-0.207141
H	-4.688644	-0.050760	0.661395
O	0.091943	-4.261938	0.292541
H	0.163768	-4.587940	1.202603

$[\{Nb_6Cl^i_{12}\}$*trans*-$Cl^a_2(H_2O)^a_4]$

Nb	0.017406	-2.216251	0.036829
Nb	0.233674	-0.055596	2.048731
Cl	0.259735	-2.484838	2.521405
Cl	0.282440	2.376172	2.507516
Cl	-2.467691	-2.478817	0.281206
Cl	2.500087	-2.502938	-0.206481
Cl	-2.174492	-0.042535	2.731054
Nb	-1.990949	-0.050531	0.236984
Nb	-0.179238	-0.065143	-1.987626
Cl	-2.673296	-0.054214	-2.171200
Cl	2.228921	-0.078198	-2.669955
Cl	-2.445679	2.382197	0.267585
H	0.037019	-0.815901	4.855471
H	-4.790425	0.736999	0.051163
H	4.844817	-0.857799	0.009843
Nb	0.036994	2.095535	0.024282
Cl	-0.205312	2.364096	-2.460286
Cl	-0.228021	-2.496917	-2.446415
Cl	2.522095	2.358079	-0.220099
H	0.017979	0.694836	-4.794426
Cl	2.727726	-0.066539	2.232290
Nb	2.045364	-0.070210	-0.175890
O	0.500333	-0.049871	4.474944
H	0.056783	0.730986	4.848852
O	4.471532	-0.081905	-0.442840
H	4.852973	0.689212	0.011190
H	-4.798538	-0.810013	0.049981
O	-0.445861	-0.070842	-4.413838
H	-0.002824	-0.852036	-4.787654
O	-4.417120	-0.038837	0.503930
Cl	0.048224	4.557595	0.017203
Cl	0.006167	-4.678317	0.043916

$[\{Nb_6Cl^i_{12}\}(OH_2)^a_5(OH)^a_1]^{1+}$

Nb	0.386669	-2.143016	0.118369
Nb	0.182153	0.044622	2.144927
Nb	-1.973894	-0.347950	0.268535
Nb	-0.124528	-0.030863	-1.927363
Nb	-0.302833	2.016741	0.097944
Nb	2.043269	0.318246	-0.049185
Cl	0.594065	-2.341126	2.629120
Cl	-0.173242	2.489785	2.540969
Cl	-1.995687	-2.825832	0.318796
Cl	2.893433	-1.998892	-0.074434
Cl	-2.210045	-0.347149	2.750587
Cl	-2.583525	-0.426478	-2.150080
Cl	2.265763	0.353443	-2.530149
Cl	-2.787522	2.012862	0.293092
Cl	-0.560842	2.397135	-2.359299
Cl	0.206927	-2.431649	-2.387076
Cl	2.051808	2.816067	-0.104681
Cl	2.632842	0.444035	2.375122
H	-0.331367	4.884822	0.817090
H	1.049374	0.662961	4.898540
H	-4.909193	-0.115219	0.018320
H	4.949577	-0.039533	0.017108
H	-0.338947	-0.907535	-4.729408
O	0.301264	0.146695	4.552532
H	0.375427	-0.727851	4.972847
O	4.415179	0.745702	-0.195857
H	4.709097	1.019625	-1.081833
O	-0.741453	4.387672	0.089026
H	-0.482874	4.853077	-0.724518
O	-0.260290	-0.021393	-4.335340
H	-0.989586	0.498998	-4.712772
O	-4.339825	-0.786340	0.431683
H	-4.665823	-0.875737	1.343796
O	0.820163	-4.078267	0.118822
H	0.127609	-4.755482	0.162606

$[\{Nb_6Cl^i_{12}\}$*trans*-$(OH)^a_2(OH_2)^a_4]^0$

Nb	0.194028	-2.153268	0.198519
Nb	0.113874	0.109358	2.124816
Nb	-1.987134	-0.156061	0.191619
Nb	-0.059303	-0.075735	-1.918772
Nb	-0.116236	2.158829	0.013368
Nb	2.056027	0.129535	0.009315
Cl	0.303081	-2.292022	2.722661
Cl	-0.029743	2.558515	2.508390
Cl	-2.261163	-2.630355	0.335129
Cl	2.719217	-2.263864	0.082922
Cl	-2.334830	-0.052883	2.671824
Cl	-2.543427	-0.278934	-2.253633
Cl	2.380016	0.047909	-2.481803
Cl	-2.659408	2.240417	0.100554
Cl	-0.259556	2.345869	-2.483645
Cl	0.071883	-2.530951	-2.315463
Cl	2.368515	2.585694	-0.151238
Cl	2.594766	0.287968	2.449946
H	0.498751	1.126687	4.812855
H	-4.792171	0.541190	0.177498
H	4.837113	-0.600733	-0.305452
H	-0.196419	-1.106983	-4.610229
O	0.189958	0.235107	4.574492
H	0.876900	-0.370068	4.902485
O	4.506412	0.290535	-0.095535
H	4.745707	0.836394	-0.864212
O	-0.261635	4.165119	0.035728
H	-0.228797	4.628260	-0.814822
O	-0.153784	-0.163144	-4.374203
H	-1.007598	0.204224	-4.661356
O	-4.439385	-0.359739	0.287206
H	-4.676688	-0.608360	1.197601
O	0.449327	-4.147205	0.275009
H	-0.333788	-4.693951	0.439172

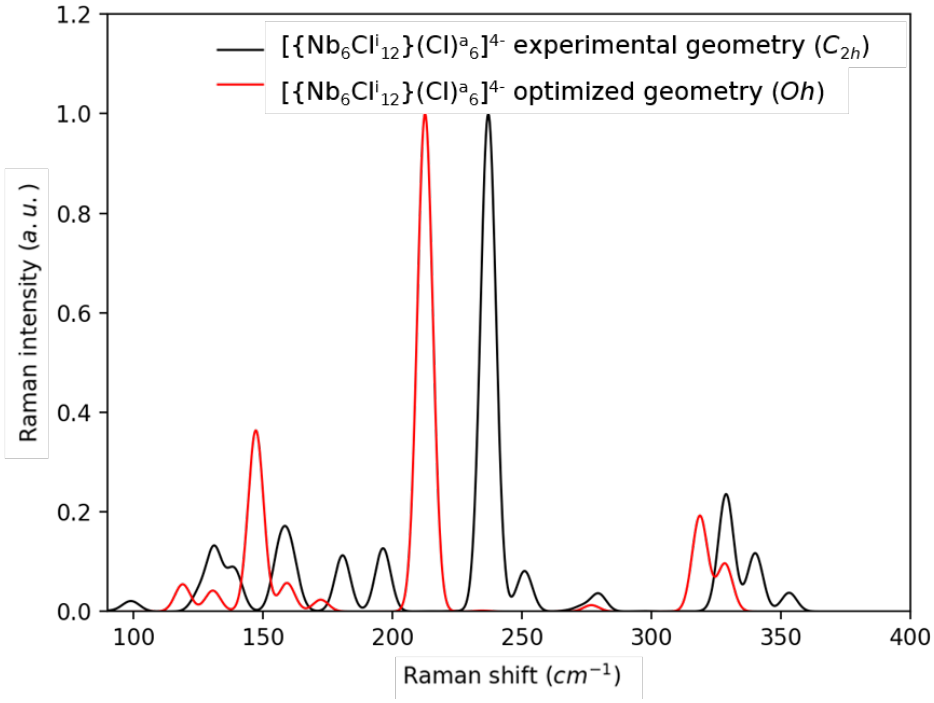

Figure S10. Normalized simulated Raman spectra obtained using the geometry issued from the X-ray structure (C_{2h}) and the optimized geometries of $[\{Nb_6Cl^i_{12}\}Cl^a_6]^{4-}$ (O_h).

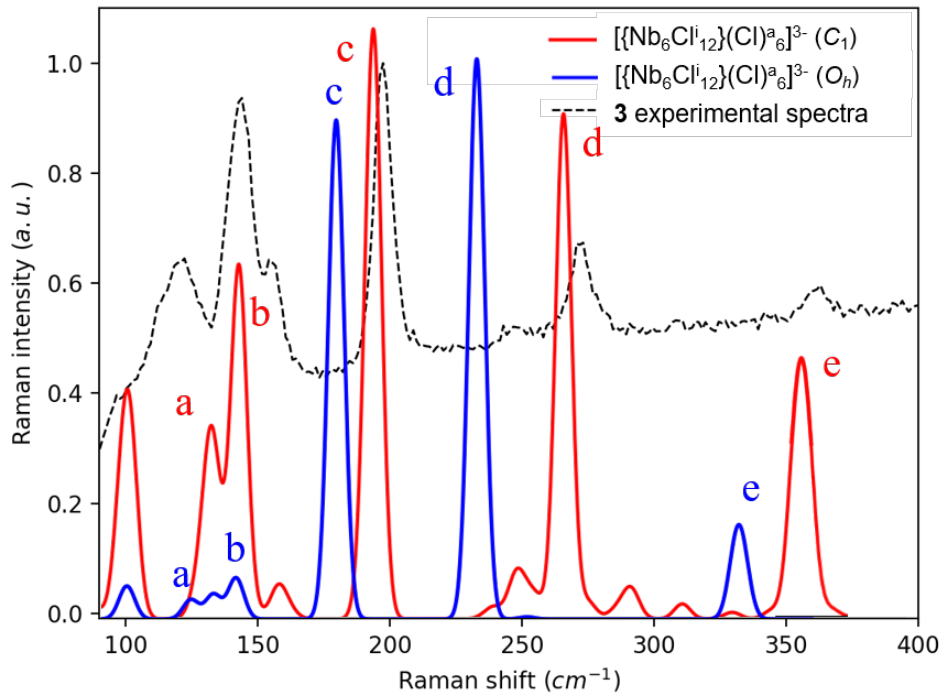

Figure S11. Normalized simulated Raman spectra of $[\{Nb_6Cl^i_{12}\}Cl^a_6]^{3-}$ (O_h symmetry and from experimental data) compared to **3** experimental spectrum.

Table S9. TD-DFT vertical electronic singlet-singlet excitation energies (eV) which oscillator strength (*f*) is superior to 0.01, wavelength (nm), and composition for $[\{Nb_6Cl^i_{12}\}Cl^a_6]^{n-}$ (n = 2-4), $[\{Nb_6Cl^i_{12}\}(H_2O)^a_6]^{2+}$, $[\{Nb_6Cl^i_{12}\}(H_2O)^a_5(OH)^a]^{+}$, and $[\{Nb_6Cl^i_{12}\}(H_2O)^a_4(OH)^a_4]$.

$[\{Nb_6Cl^i_{12}\}Cl^a_6]^{2-}$				
Electronic excitation energy (eV)	λ (nm)	*f*	**Composition**	
1.076	1152	0.006	HOMO-1→LUMO	87%
2.436	509	0.049	HOMO-6→LUMO	54%
			HOMO-1→LUMO+3	36%
2.500	496	0.096	HOMO-1→LUMO+3	46%
			HOMO-6→LUMO	40%
2.950	421	0.069	HOMO-3→LUMO+3	83%
4.558	272	0.022	HOMO→LUMO+4	93%

$[\{Nb_6Cl^i_{12}\}Cl^a_6]^{3-}$				
Electronic excitation energy (eV)	λ (nm)	*f*	**Composition**	
0.998	1242	0.008	HOSOα→LUSOα+1	83%
			HOSOβ-3→LUSOβ	10%
1.175	1055	0.010	HOSOβ-3→LUSOβ	84%
			HOSOα→LUSOα+1	14%
2.627	472	0.130	HOSOα-2→LUSOα+3	72%
2.837	437	0.005	HOSOα-5→LUSOα+1	98%

$[\{Nb_6Cl^i_{12}\}Cl^a_6]^{4-}$				
Electronic excitation energy (eV)	λ (nm)	*f*	**Composition**	
1.385	895	0.037	HOMO→LUMO	94%
2.761	449	0.111	HOMO-2→LUMO+2	66%
			HOMO-1→LUMO+3	8%
			HOMO-1→LUMO+8	6%
3.046	407	0.033	HOMO-1→LUMO+3	90%
3.163	392	0.030	HOMO-4→LUMO+2	83%
			HOMO-6→LUMO	8%

$[Nb_6Cl_{12}(H_2O)_6]^{2+}$				
Electronic excitation energy (eV)	**λ (nm)**	**f**	**Nature**	
1.514	819	0.014	HOMO→LUMO	60%
			HOMO→LUMO+1	19%
			HOMO→LUMO+2	11%
1.525	813	0.014	HOMO→LUMO+1	56%
			HOMO→LUMO	26%
			HOMO→LUMO+2	4%

1.533	809	0.014	HOMO→LUMO+2	74%
			HOMO→LUMO+1	11%
3.115	398	0.019	HOMO-6→LUMO+6	18%
			HOMO-4→LUMO+4	18%
			HOMO-5→LUMO+3	17%
			HOMO-3→LUMO+8	13%
			HOMO-2→LUMO+8	11%
3.131	396	0.018	HOMO-4→LUMO+5	21%
			HOMO-6→LUMO+3	17%
			HOMO-3→LUMO+8	10%
			HOMO-1→LUMO+8	10%
			HOMO-5→LUMO+7	9%
			HOMO-1→LUMO+9	8%
3.147	394	0.018	HOMO-5→LUMO+5	22%
			HOMO-6→LUMO+4	19%
			HOMO-2→LUMO+9	18%
			HOMO-1→LUMO+9	12%
			HOMO-4→LUMO+7	10%
3.324	373	0.009	HOMO-3→LUMO+8	28%
			HOMO-1→LUMO+9	26%
			HOMO-6→LUMO+3	8%
			HOMO-4→LUMO+5	8%

$[Nb_6Cl_{12}(H_2O)_5(OH)]^+$				
Electronic excitation energy (eV)	**λ (nm)**	***f***	**Nature**	
1.427	869	0.008	HOMO→LUMO	73%
			HOMO→LUMO+1	12%
1.571	789	0.013	HOMO→LUMO+2	87%
2.003	619	0.008	HOMO→LUMO+6	50%
			HOMO-1→LUMO	22%
			HOMO→LUMO+1	20%
2.818	440	0.007	HOMO-6→LUMO	23%
			HOMO-5→LUMO+3	18%
			HOMO-6→LUMO+2	12%
			HOMO-1→LUMO+8	10%
			HOMO-1→LUMO+9	9%
3.069	404	0.012	HOMO-2→LUMO+10	36%
			HOMO-6→LUMO+3	30%
			HOMO-5→LUMO+7	8%
3.092	401	0.012	HOMO-2→LUMO+10	20%
			HOMO-6→LUMO+3	17%
			HOMO-1→LUMO+8	11%
			HOMO-6→LUMO+4	7%
3.107	399	0.012	HOMO-6→LUMO+6	30%
			HOMO-5→LUMO+5	10%
			HOMO-2→LUMO+8	10%
			HOMO-6→LUMO+1	6%

4.335	286	0.009	HOMO-13→LUMO	35%
			HOMO-9→LUMO+7	20%
			HOMO-11→LUMO+7	13%
			HOMO-3→LUMO+19	10%

$[Nb_6Cl_{12}(H_2O)_4$*trans*$-(OH)_2]$				
Electronic excitation energy (eV)	**λ (nm)**	***f***	**Nature**	
1.406	882	0.011	HOMO→LUMO	93%
1.660	747	0.009	HOMO→LUMO+4	42%
			HOMO→LUMO+2	22%
			HOMO-1→LUMO	13%
1.666	744	0.008	HOMO→LUMO+5	30%
			HOMO→LUMO+3	22%
			HOMO-2→LUMO	21%
			HOMO-1→LUMO+1	10%
2.567	483	0.017	HOMO-6→LUMO+1	27%
			HOMO-5→LUMO+4	23%
			HOMO-4→LUMO+5	12%
			HOMO-4→LUMO+7	6%
2.761	449	0.013	HOMO-6→LUMO+1	36%
			HOMO-7→LUMO+1	18%
			HOMO-6→LUMO+2	8%
			HOMO-6→LUMO+4	8%
2.792	444	0.014	HOMO-6→LUMO+2	27%
			HOMO-4→LUMO+1	13%
			HOMO-1→LUMO+10	10%
			HOMO-6→LUMO+4	8%
			HOMO-7→LUMO+1	8%
2.960	419	0.008	HOMO-7→LUMO+4	39%
			HOMO-6→LUMO+4	16%
			HOMO-4→LUMO+6	6%
3.280	378	0.010	HOMO-5→LUMO+10	58%
			HOMO-4→LUMO+9	20%
4.065	305	0.014	HOMO-1→LUMO+22	9%
			HOMO-3→LUMO+15	8%
			HOMO-2→LUMO+21	6%
			HOMO-3→LUMO+20	6%
			HOMO-11→LUMO+1	6%
			HOMO-3→LUMO+19	6%
			HOMO-2→LUMO+23	5%

REFERENCES

(1) Simon, A. *et al.* $K_4Nb_6Cl_{18}$ - Darstellung, Eigenschaften und Struktur *Zeit. Anorg. Allg. Chem.* **1968**, *361*, 235–248.

(2) Fleming, P. B. *et al.* Chemistry of polynuclear metal halides. II. Preparation of polynuclear niobium chloride and bromide *Inorg. Chem.*, **1967**, *6*, 1–4.

(3) Parsons, J. A. *et al.* High temperature conproportionation of niobium pentahalide and niobium metal; A convenient route to hydrated cluster halides $Nb_6Cl_{14}\cdot 8H_2O$ and $Nb_6Br_{14}\cdot 8H_2O$ *Inorg. Nucl. Chem. Lett.*, **1972**, *8*, 281–286.

(4) Koknat, F. W. *et al.* Metal Cluster Halide Complexes. I. Efficient Synthesis of Hydrated Hexanuclear Niobium and Tantalum Cluster Halides $M_6X_{14}\cdot 8H_2O$. *Inorg. Chem.* **1974**, *13*, 1699–1702.

(5) Schäfer, H. *et al.* Die Niob- und Tantalkomplexe $[Me_6X^i_{12}]X^a_2.nH_2O$ mit Me=Nb, Ta; Xi=Cl, Br; Xa=Cl, Br, J. *Zeit. Anorg. Allg. Chem.* **1972**, *392*, 10–22.

(6) Schäfer, H. *et al.* Das chemische Verhalten von Me_6-Komplexen (Me=Nb, Ta, Mo, W) aus analytischer Sicht. *Zeit. Anorg. Allg. Chem.* **1973**, *401*, 63–84.

(7) Quigley, R. *et al.* Electrochemical and Spectroscopic Characterization of $\{Nb_6Cl_{12}\}^{z+}$Chloride Clusters in the Aluminum Chloride-l-Methyl-3-ethylimidazolium Chloride Molten Salt. *Inorg. Chem.* **1992**, *31*, 1255–1261.

(8) Pénicaud, A. *et al.* Novel Redox Properties of the Paramagnetic Hexanuclear Niobium Cluster Halide $Nb_6Cl_{18}^{3-}$ and the Preparation, Structures, and Conducting and Magnetic Properties of Its One-Dimensional Mixed-Valence Tetramethyltetra(selena and thia)fulvalenium Salts: [TMTSF. *Chem. Mater.* **2**, 123–132 (1990).

(9) Prokopuk, N. *et al.* Synthesis and structure of the useful starting material $[Bu_4N]_3[Nb_6Cl_{12}(OSO_2CF_3)_6]$. *Inorganica Chim. Acta* **2000**, *300–302*, 951–957.

(10) Rodríguez-Carvajal, J. Recent advances in magnetic structure determination by neutron powder diffraction. *Phys. B Phys. Condens. Matter* **1993**, *192*, 55–69.

(11) Roisnel, T. *et al* WinPLOTR: A Windows tool for powder diffraction pattern analysis. *Epdic 7 Eur. Powder Diffraction, Pts 1 2* **378**, 118–123 (2001).

(12) Fonseca Guerra, C. *et al* Towards an order-N DFT method. *Theor. Chem. Acc.* **1998**, *99*, 391–403.

(13) te Velde, G. *et al.* Chemistry with ADF. *J. Comput. Chem.* **2001**, *22*, 931–967.

(14) Vosko, S. H. *et al* Accurate spin-dependent electron liquid correlation energies for local spin density calculations: a critical analysis. *Can. J. Phys.* **1980**, *58*, 1200–1211.

(15) Zhang, Y. *et al* Comment on "generalized gradient approximation made simple". *Phys. Rev. Lett.* **1998**, *80*, 890.

(16) Van Lenthe, E. Geometry optimizations in the zero-order regular approximation for relativistic effects. *J. Chem. Phys.* **1999**, *110*, 8943–8953.

(17) Van Lenthe, E. *et al.* Optimized Slater-type basis sets for the elements 1-118. *J. Comput. Chem.* **2003**, *24*, 1142–1156.

(18) Costuas, K. *et al.* Combined theoretical and time-resolved photoluminescence investigations of $[Mo_6Br^i_8Br^a_6]^{2-}$ metal cluster units: Evidence of dual emission. *Phys. Chem. Chem. Phys.* **2015**, *17*, 28574–28585.

(19) Kepenekian, M. *et al.* Red-NIR luminescence of Mo_6 monolayered assembly directly anchored on Au(001). *Mater. Horizons* **2019**, *6*, 1828–1833.